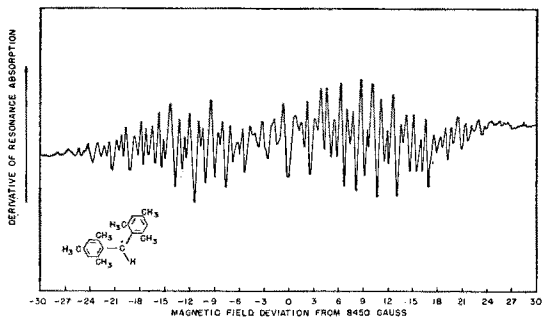

FIG. 2. Derivative of the paramagnetic resonance absorption spectrum of dimesitylmethyl.

if the reduction of the number of hydrogen atoms attached to the phenyl rings gives a simpler resonance spectrum. Since the ortho- and para-positions on the phenyl rings contain methyl groups, the hyperfine structure would be expected to arise entirely from the four meta-hydrogens. There would then be five hyperfine structure lines with a Gaussian intensity distribution. If there is in addition a large methyl hydrogen splitting, a spectrum of two sets of five lines each should be observed. The measured spectrum (Fig. 2) does not conform with this simple expectation. It is apparent that although there are indeed two sets of peaks separated by 24 oersteds, each set contains many more than five lines. Molecular orbital calculations assuming a planar molecule indicate that because of hyperconjugation the electron density on the para-methyl group is greater by a factor of 400 than the density on the ortho-methyl groups. If this is true, the hydrogen nuclei of the para-methyl groups would exist in the π-electron system and a large hyperfine coupling with the unpaired electron would result. If the hydrogen atoms of the para-methyl groups are assumed to be equivalent, each of the hyperfine structure peaks discussed above would be split into seven peaks to give for the whole spectrum two sets of 35 peaks each. This result is in qualitative agreement with the spectrum shown in Fig. 2.

The authors wish to thank Dr. R. E. Merrifield of this laboratory for carrying out the molecular orbital calculations on dimesitylmethyl.

* Present address: 2nd Army Area Med. Lab., Ft. Geo. G. Meade, Maryland.

Stability and Structure of Bunsen Flame*

MAHINDER S. UBEROI
Department of Aeronautical Engineering, University of Michigan, Ann Arbor, Michigan
(Received August 6, 1954)

A LEAN propane-air flame was established on $\frac{3}{4}$-in. diameter tube and the flow upstream of the flame was made uniform by using a number of very fine screens. As the volume flow was decreased at constant mixture ratio the tip of the flame changed from concave to convex (see Fig. 1). The following is offered as a tentative explanation of the phenomenon.

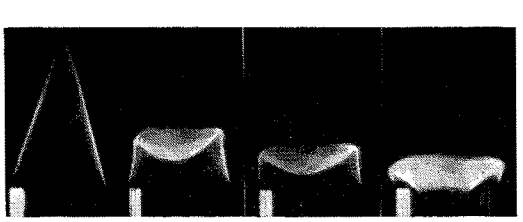

FIG. 1. Change of flame shape with decreasing volume flow (from left to right).

Far upstream of the flame the unburned gas flow is parallel and the flow bends away from the burner axis before reaching the flame. Since the velocity component normal to the flame is increased considerably after combustion and the flame is concave towards the unburned gas, the burned gases are further bent away from the burner axis. Assuming constant flame speed the pressure drop across the flame is the same for every streamline and there is no pressure drop towards the burner axis to make the diverging flow parallel. For a flame convex towards the unburned gas, the flow also bends away from the burner axis before reaching the flame but after going through the flame the burned gases are bent towards the burner axis. The pressure is higher in the central than in the outer streamlines and this bends the streamlines away from the center. An equilibrium is reached further downstream where the flow becomes parallel and pressure becomes uniform.

In practice the concave Bunsen burner flame is realized because the flame speed increases as we go from the base to the tip of the flame; i.e., going through the flame the central streamlines experience more pressure drop than the outer streamlines. This pressure drop toward the center makes the diverging burned gases parallel. As the height of the flame decreases the curvature decreases and change in flame speed at the tip is not big enough to support a concave flame. These considerations apply quite generally but it is not possible to demonstrate this for the usual Bunsen burner. The usual burner has a boundary layer at the wall (in the above experiment we decreased this considerably by using very fine screens) and the flame flashes back at the rim before the volume flow is low enough for the flame curvature to change at the tip.

In view of the above considerations, the usual assumption that the shape of the Bunsen burner flame and the flow field can be determined by assuming constant flame speed is untenable. Other theoretical considerations and detail flow field measurements supporting these views will be reported elsewhere.

* This work is a part of the research program supported by the U. S. Office of Naval Research under Contract NONR 1224-02.

Mass Spectrometric Detection of Free OH Radical in the Thermal Decomposition Products of H_2O Vapor

T. TSUCHIYA
Tokyo Chemical Industrial Research Institute, 58, 1, Nakameguro, Tokyo, Japan
(Received July 14, 1954)

SEVERAL methods have been reported in the past for the detection of the free hydroxyl radical OH: and these were recently re-examined by the microwave spectral method.[1] Consequently, it has become apparent that of these methods only the one in which the intensity of the OH absorption spectrum is measured in the ultraviolet region can give satisfactory results.

In an experiment preliminary to the series in our research on the mechanism of thermal decomposition of gas molecules, free OH radicals were detected with the mass spectrometer by subjecting H_2O vapor to pyrolysis on a platinum filament.

The work was carried out with a 60° or Nier type mass spectrometer made by the Scientific Research Institute.[2] A small auxiliary platinum filament similar to that described by Robertson[3] was installed in the ionization chamber for the pyrolysis of gas molecules. The temperature of this filament was measured with an optical pyrometer. Throughout the experiment the heating temperature was 1200°C. Electron energies were measured with a calibrated dc meter capable of being read to an accuracy of 0.1 percent of full scale reading. The H_2O was an ordinary distilled

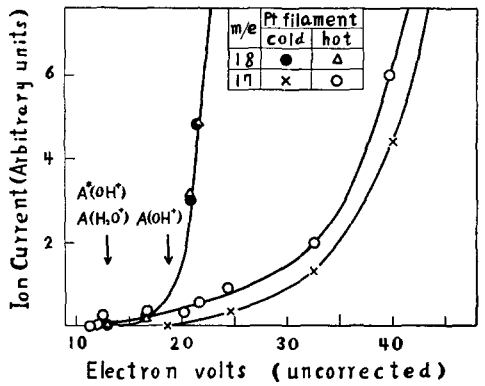

FIG. 1. Ionization efficiency curves for $m/e=17$ and 18, with hot and cold Pt filaments, small background spectra included.

sample, and was introduced into the ionization chamber as a molecular beam.

Heating of the Pt filament produces the following effects on the mass spectra of H_2O.

1. The appearance potential of OH^+ ions decreases from its normal value of $A(OH^+)=18.7$ ev[4] to a new value $A^*(OH^+)$ which is nearly equal to the appearance potential of the parent ion, $A(H_2O^+)=13.0$ ev[4] (Fig. 1).
2. The appearance potential of H^+ also decreases by roughly about 2 ev.
3. As seen in Fig. 1, practically no change at all occurs in the H_2O^+ ionization efficiency curve.
4. Under ordinary operating conditions, electron energy at 70 ev, the ratio of intensities N, of $m/e=17$ ions to $m/e=18$ ions, is always larger than when measured with an unheated Pt filament. In one example cold filament value of $N=0.35$ increased to 0.63 after heating the Pt filament for one minute.
5. At $m/e=16$, a spectrum appears: the ratio of its intensity to that of H_2O^+ is about 1/10.
6. Turning off the electron current and using just the heated Pt filament alone produces no H_2O spectra at all

Effect 3 gives no indication of the presence of excited H_2O molecules.

From the hot Pt filament curve I in Fig. 2, it is seen that near $A(OH^+)$, where the cold filament curve II becomes zero, the amount of OH^+ shows a markedly uniform and continuous increase relative to that of H_2O^+, as the electron energy is lowered.

In accordance with these facts and effects 4, 5 and 6, we can

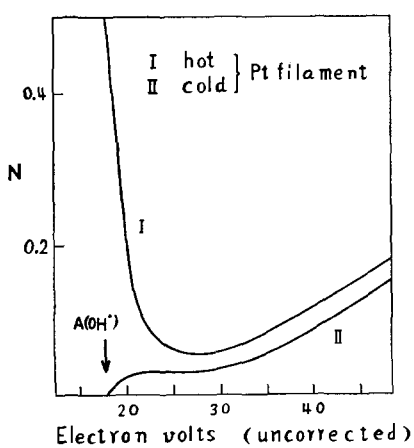

FIG. 2. Intensity ratio N between the $m/e=17$ spectrum and the $m/e=18$ spectrum, *vs* electron energy.

reasonably expect that new particles such as free OH radicals are being formed thermally.[5] Taking into account effects 2 and 6, the main decomposition mechanism would be $H_2O \rightarrow OH+H$.

The ionization potential $I(OH)$ of the OH radical is reported to be ≤ 13.6 ev.[4] Neglecting the small effects due to vertical transition favored by the Franck-Condon principle[6] and the possibility of thermally produced OH radicals being in excited states, $A^*(OH)$ equals $I(OH)$. Again from consideration of this appearance potential, effect 1, namely that $A^*(OH^+)$ nearly equals $A(H_2O^+)=13.0$ ev, can also be explained beautifully by assuming free OH radicals to be present.

Precise measurement of the appearance potential of the OH radical is now in progress.

[1] Sanders, Schawlow, Dousmanis, and Townes, J. Chem. Phys. **22**, 245 (1954).
[2] Nishina Research Laboratory, Kagaku Kenkyujo Hokoku, **27**, 435 (1951). In Japanese.
[3] A. J. B. Robertson, Proc. Roy. Soc. (London) **A199**, 394 (1949).
[4] Mann, Hustrulid, and Tate, Phys. Rev. **58**, 340 (1940).
[5] G. C. Eltenton, J. Chem. Phys. **15**, 455 (1947).
[6] R. E. Honig, J. Chem. Phys. **16**, 105 (1948).

Note on the Hybrids in the Nontetrahedral Carbon Atom

M. MASHIMA
Faculty of Liberal Arts, Saga University, Saga, Japan
(Received July 28, 1954)

THE hybrid orbitals in the nontetrahedral carbon atom have been investigated by a number of authors.[1-5] Coulson and Moffitt[3] especially have given an exact treatment of the bent bonds in some strained hydrocarbons. However, Kilpatrick and Spitzer's[2] criterion for the bent bonds was improved here.

With no loss in generality, bonding orbitals in a quadrivalent carbon atom are formed as follows:[2]

$$f_1=as+bp_z+(1/2)^{\frac{1}{2}}p_x,$$
$$f_2=as+bp_z-(1/2)^{\frac{1}{2}}p_x,$$
$$f_3=bs-ap_z+(1/2)^{\frac{1}{2}}p_y,$$
$$f_4=bs-ap_z-(1/2)^{\frac{1}{2}}p_y,$$
$$b=+(1/2-a^2)^{\frac{1}{2}}.$$

The equivalent orbitals f_1 and f_2 are used to form the two C−C bonds, and have their maximum values in the XZ plane. f_3 and f_4 (taken in the YZ plane) are equivalent. The bond strength of f_1 is given by the expression:

$$S=a+(1/2-a^2)^{\frac{1}{2}}3^{\frac{1}{2}}\cos\theta+(3/2)^{\frac{1}{2}}\sin\theta. \quad (1)$$

The condition $dS/da=0$ now being used, the following relations are obtained:[2]

$$a=(1/2+6\cos^2\theta_0)^{\frac{1}{2}}, \quad b=(3\cos^2\theta_0/2+6\cos^2\theta_0)^{\frac{1}{2}},$$

where θ_0 is not an angle at which S has the maximum value, but equated to θ which is contained in the equation obtained by $dS/da=0$. Thus Eq. (1) becomes as follows:

$$S=(1/2+6\cos^2\theta_0)^{\frac{1}{2}}+(3\cos^2\theta_0/2+6\cos^2\theta_0)^{\frac{1}{2}}3^{\frac{1}{2}}\cos\theta + (3/2)^{\frac{1}{2}}\sin\theta. \quad (2)$$

By setting $\theta=\theta_0$ in Eq. (2), f_1 has a value a particular direction θ_0. But it has the maximum value in a direction θ differing from θ_0. The angular dependence of the bond strength of f_1 at $\theta_0=30°$ is shown in Fig. 1.

As the measure of binding power, Kilpatrick and Spitzer[2] have used $S\theta_0$ which is the numerical value of S in the bond direction. However, it is evident from Fig. 1 that the cosine of S in the bond direction has the greatest value at any angle $\theta_0+\beta$. (β is an angle between new direction and bond direction.) The numerical value of $S\cdot\cos\beta(=S_\beta)$ is given by the expression:

$$S_\beta=\cos\beta\{a+(1/2-a^2)^{\frac{1}{2}}3^{\frac{1}{2}}\cos(\beta+\alpha/2)+(3/2)^{\frac{1}{2}}\sin(\beta+\alpha/2), \quad (3)$$